Scientific Research Publishing

Open Journal of Fluid Dynamics, 2023, 13, 104-112
https://www.scirp.org/journal/ojfd
ISSN Online: 2165-3860
ISSN Print: 2165-3852

Study on Collision Process of Opposing Unsteady Supersonic Jets and Shock Waves

Sakira Uno[1], Hiroshi Fukuoka[2*], Atsushi Suda[2], Ikurou Umezu[3]

[1]Faculty of Advanced Engineering, National Institute of Technology, Nara College, Yamatokoriyama, Nara, Japan
[2]Department of Mechanical Engineering, National Institute of Technology, Nara College, Yamatokoriyama, Nara, Japan
[3]Department of Physics, Konan University, Kobe, Japan
Email: *fukuoka@mech.nara-k.ac.jp

How to cite this paper: Uno, S., Fukuoka, H., Suda, A. and Umezu, I. (2023) Study on Collision Process of Opposing Unsteady Supersonic Jets and Shock Waves. *Open Journal of Fluid Dynamics*, **13**, 104-112.
https://doi.org/10.4236/ojfd.2023.132008

Received: March 20, 2023
Accepted: May 22, 2023
Published: May 25, 2023

Abstract

Double pulsed-laser-ablation is a promising method to prepare nanoparticle composites. The backward movement of the plume after the collision with counter-propagating shock wave has been observed in experiments. In the present study, collision dynamics of the oppositely injected Si and Ge jets into a He background gas was numerically calculated as a simulation for double pulsed-laser-ablation. The experimentally observed backward movement was reproduced. The effect of distance between two jet exits on the distance of backward movement of the jet, B_L, after the collision with the counter-propagating shock front was calculated to discuss the collision dynamics and to optimize the target distance for the experiment. We found that B_L does not decrease monotonically with increasing distance between two jet exits, but has a maximum value at a certain distance. This behavior is discussed by calculating the expansion dynamics of an individual jet. Shock wave grows with time at the initial stage of the jet expansion and then attenuates; the density just behind the shock front for individual jet has a maximum value at a certain time and position. B_L has a maximum value when the densities just behind the shock fronts for the individual jets have maximum values. This result is important for designing the appropriate distance between the two jet exits, *i.e.*, the distance between the targets of double pulsed-laser-ablation.

Keywords

Collision of Supersonic Jets, Shock Wave, Computational Fluid Dynamics, Laser Ablation

1. Introduction

Pulsed laser ablation (PLA) in a background gas is a method to prepare nano-

particles [1] [2]. Irradiation of the strong pulsed laser on the solid surface induces the ejection of vapor called a plume. Shock wave is formed during the expansion of the plume and it plays an essential role in plume expansion dynamics [3] [4]. Nanoparticles are formed during plume cooling [5]. Recently, PLA with two lasers and two targets was proposed to prepare nanoparticle composites. This method is called double pulsed-laser-ablation (DPLA). In the case of DPLA, not only the effect of the shock wave propagating just in front of the plume but also the counter-propagating shock wave is important for plume expansion dynamics. For example, the backward movement of the plume after the collision with the counter-propagating shock front is experimentally observed in DPLA [6] [7].

The effects of the counter-propagating shock wave on the plume can be simulated by replacing the plume with the unsteady supersonic jet. The change in the plume expansion direction [8] and the backward movement of the plume [7] after the collision of the two shock waves have been discussed by this method. The advantages of the calculation are that quantitative analysis is possible and initial conditions can be set freely. However, quantitative discussion was not enough and initial conditions were not changed in the previous reports. The effect of distance between two targets is important for DPLA since plume expansion dynamics depends on the distance from the target surface. The results of the calculations are also important to estimate the optimal distance between targets. In the present paper, distance of backward movement of the jets after the collision with the counter-propagating shock waves is calculated by varying the distance between two jet exits, and the effect of collision on the backward movement is quantitatively discussed.

2. Computational Method

2.1. Governing Equations and Numerical Procedure

The expansion dynamics of the oppositely injected Si and Ge jets into a He background gas was numerically simulated. Axisymmetric two-dimensional compressible Euler equation and conservation equations of mass and total energy were used as the governing equations. The equations are written as:

$$\frac{\partial \boldsymbol{U}}{\partial t}+\frac{\partial \boldsymbol{F}}{\partial x}+\frac{\partial \boldsymbol{G}}{\partial r}+\boldsymbol{H}=0\,. \tag{1}$$

where t, x and r are time, coordinate in the symmetrical axis and that in the radial axis, respectively. The symbols of $\boldsymbol{U}$, $\boldsymbol{F}$, $\boldsymbol{G}$ and $\boldsymbol{H}$ are conservative quantity vector, physical flux vector in x coordinate, that in r coordinate and source term, respectively. They consist of density, ρ, velocity in the x coordinate, u, that in the r coordinate, v, pressure, p and total energy per unit volume, e. The densities of Si, Ge and He species are distinguished by the subscripts s, g and h, respectively, in the conservation equations of mass. Relationships between those vectors and quantities are expressed as Equation (2). Since all gas species are assumed to be the ideal gases, quantities of ρ, u, v, p, e and specific heat ratio, γ, obey Equation

(3).

$$\boldsymbol{U}=\begin{pmatrix}\rho_s\\ \rho_g\\ \rho_h\\ \rho u\\ \rho v\\ e\end{pmatrix},\boldsymbol{F}=\begin{pmatrix}\rho_s u\\ \rho_g u\\ \rho_h u\\ \rho u^2+p\\ \rho uv\\ (e+p)u\end{pmatrix},\boldsymbol{G}=\begin{pmatrix}\rho_s v\\ \rho_g v\\ \rho_h v\\ \rho uv\\ \rho v^2+p\\ (e+p)v\end{pmatrix},\boldsymbol{H}=\frac{1}{r}\begin{pmatrix}\rho_s v\\ \rho_g v\\ \rho_h v\\ \rho uv\\ \rho v^2\\ (e+p)v\end{pmatrix}. \quad (2)$$

$$e=\frac{p}{\gamma-1}+\frac{\rho}{2}\left(u^2+v^2\right). \quad (3)$$

The numerical calculations were performed by ANSYS Fluent 14.0.0 code using the finite volume method. The density-based solver was used to simulate the supersonic flow. The governing equations were spatially discretized by the explicit method. A fourth-order Runge-Kutta scheme was used for the explicit time integration. The second-order upwind scheme and Roe's Flux-Difference Splitting scheme were used to discretize the convective term and numerical flux, respectively. A Courant-Friedrichs-Lewy condition was set at 0.1 to stabilize the calculation. Grid dependency was evaluated [8] based on the three grid sizes $D/30$, $D/20$ and $D/10$ mm, where D = 1 mm. Since the jet expansion velocities for these conditions were almost the same, a grid size of $D/10$ mm was adopted to save the calculation time. The aspect ratio of the grid was set at 1.

2.2. Boundary and Initial Conditions

The numerical calculation area and boundary conditions are shown in Figure 1. The distance from the Si jet exit along the vertical direction, that along the horizontal direction, the jet exit diameter and the distance between two jet exits were

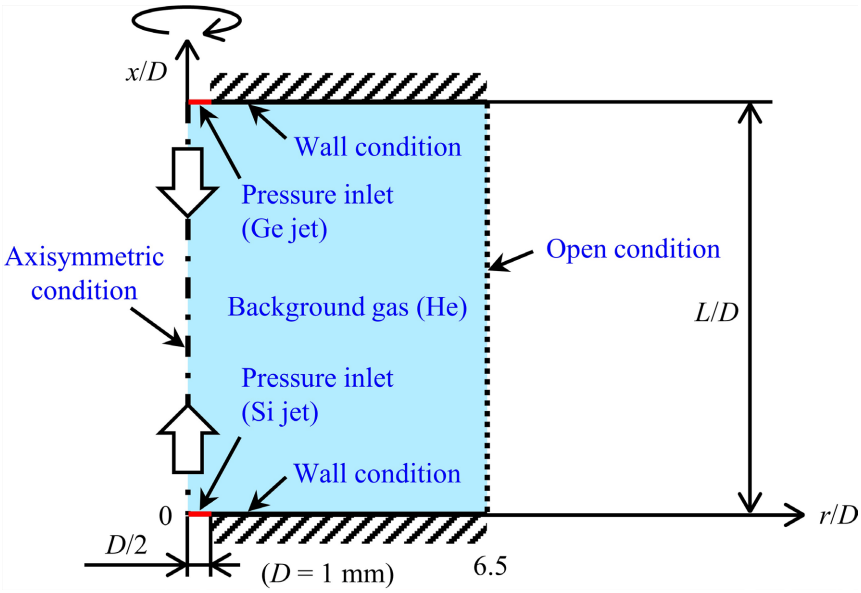

Figure 1. Arrangement of Si and Ge jet exits and walls and boundary conditions used for the numerical calculation.

denoted to x, r, D and L, respectively. Pressure inlets were applied to the positions of $x/D = 0$ and L/D as the jet exits for Si and Ge, respectively. Si and Ge jets were simultaneously injected into a He background gas at 3000 Pa and 300 K as shown by solid-white arrows in Figure 1. Slip wall conditions were applied to the lower and upper walls. Axisymmetric and open conditions were applied to the positions of $r/D = 0$ and 6.5, respectively, along the x/D direction. The initial conditions for Si and Ge jets are shown in Table 1. Injections of both jets were cut off after 27 ns. These conditions were tuned to satisfy the initial expansion speed of the laser-induced plume in the experiment. The expansions of jets are evaluated by x/D. The effect of the collision between jet and the counter-propagating shock wave is evaluated as a function of L/D. The value of L/D was varied from 7 to 18, which corresponds to varying the distance between two targets from 7 to 18 mm for DPLA when the jet exit diameter, $D = 1$ mm. Hereafter, the obtained non-dimensional values are changed to length by using $D = 1$ mm.

3. Results

3.1. Typical Flow Field

The temporal evolution of the jets and shock waves for $L = 9$ mm are shown in Figure 2. Time t is the elapsed time after the jet injection. White lines and colors in the left images of Figures 2(a)-(e) show contour lines of density and contour

Table 1. Initial conditions for Si and Ge jets.

Jet	Gauge total pressure (Pa)	Initial gauge pressure (Pa)	Specific heat ratio (–)	Gas constant (J/(kg·K))	Total temperature (K)
Si	1.82×10^7	9.12×10^5	1.61	523	3.20×10^5
Ge	1.95×10^7	9.12×10^5	1.65	339	8.20×10^5

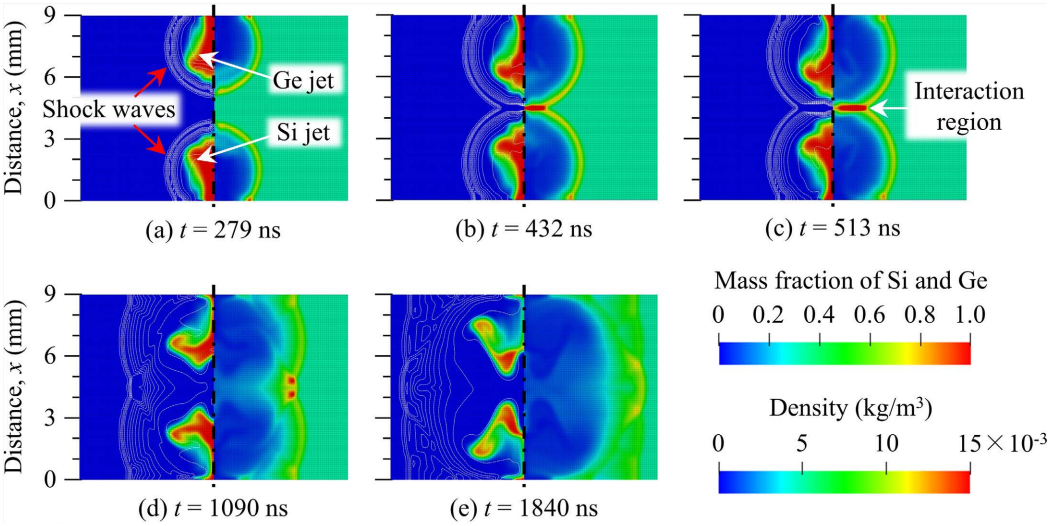

Figure 2. Evolution of jets and shock waves for $L = 9$ mm. White lines and colors in the left half show contour lines of density and contour plots of mass fraction of Si and Ge, respectively. The right half show contour plots of density.

plots of mass fraction of Si and Ge, respectively. The right images of Figures 2(a)-(e) show contour plots of density. Shock waves are formed in front of the jets at the initial stage of the expansion, as shown by the white lines in Figure 2(a). In the later stage, shock waves collide in the central region, and shock fronts propagate toward the jets, as shown in Figure 2(b) and Figure 2(c). A high-density interaction region is formed behind the shock fronts due to the collision of the shock waves, as shown in the right images of Figure 2(b) and Figure 2(c). In this interaction region, flows toward the jets are induced just behind the shock fronts due to the pressure difference across the shock fronts. The jet fronts collide with the counter-propagating shock fronts at around $t = 500$ ns as shown in Figure 2(c). After the collision with the counter-propagating shock fronts, the backward movements of the jet fronts are found, as shown in Figures 2(c)-(e). Finally, the backward movements end as described in the following subsection.

3.2. Effect of Distance between Two Jet Exits on the Backward Movement of the Jet Front

The effects of the collision depend on the distance between two jets, *i.e.*, the distance between two jet exits. We evaluated the distance of backward movement of the jet front as a degree of the effects of the collision. We analyzed the expansion dynamics of jets along the line connecting the center of two jet exits. In the present paper, we mainly discuss the expansion dynamics of the Si jet and the counter-propagating shock front, since the behavior of the Ge jet is basically the same. Figure 3 shows the temporal evolution of the jet fronts and the shock fronts for $L = 9$ mm. The blue solid and dashed lines indicate the positions of Si and Ge jet fronts, respectively, and the red lines indicate the positions of shock fronts. Si and Ge jets are injected from $x = 0$ and 9 mm, respectively. The shock fronts collide at about $t = 400$ ns. Subsequently, the interaction region, shown in

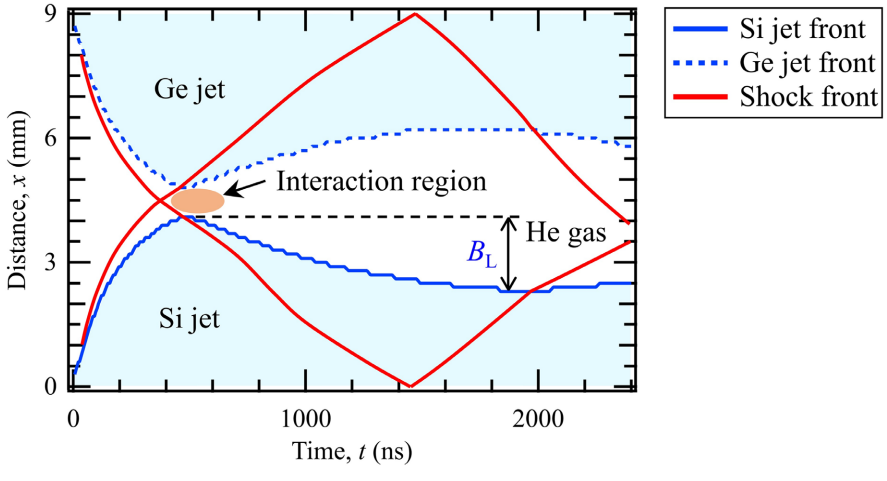

Figure 3. The temporal evolution of the jet fronts and the shock fronts for $L = 9$ mm. The blue solid and dashed lines indicate positions of Si and Ge jet fronts, respectively, and the red lines indicate positions of the shock fronts.

Figure 2(b) and Figure 2(c), is formed behind the shock fronts. Si jet front and counter-propagating shock front collide at about $t = 500$ ns and $x = 4.1$ mm. After that, the Si jet front moves backward, and the shock front propagates inside the Si jet toward the lower wall ($x = 0$ mm). The shock front reflects at the lower wall and it collides with the Si jet front again at about $t = 2000$ ns and $x = 2.3$ mm. After that, the Si jet front begins to move forward again. Here we evaluate the distance of backward movement, B_L, which is defined as the distance between positions where the Si jet front collides with the counter-propagating shock front and where it collides with the reflected shock front, as shown in Figure 3. It corresponds to the distance between the positions of the start and end of the backward movement.

The distance of backward movement, B_L, is shown in Figure 4 as a function of L which is the distance between two jet exits. If the effect of collision decreases with increasing L, B_L will decrease monotonically with L. The result of the calculation indicates that B_L has a maximum value at $L = 10.7$ mm.

4. Discussion

We calculate the density induced just behind the shock front to reveal the origin of the behavior shown in Figure 4. Hereafter, the conditions in which single (Si or Ge) jet and double (Si and Ge) jets are injected are called single-jet and double-jet condition, respectively. The density distribution for the single-jet condition for Si at $t = 560$ ns is shown in Figure 5. Si jet is injected from the jet exit placed at $x = 0$ mm and it expands along the direction shown by the red arrow. The shock front is defined as the position where the density exceeds one-tenth of the density difference between the peak (14.2×10^{-3} kg/m^3) and the initial value (4.81×10^{-3} kg/m^3), as shown by the blue dashed line in Figure 5. Furthermore, we denote the distance between the jet exit and the shock front at t as $S_{Si}(t)$ for Si for single-jet condition, as shown by the blue arrow in Figure 5.

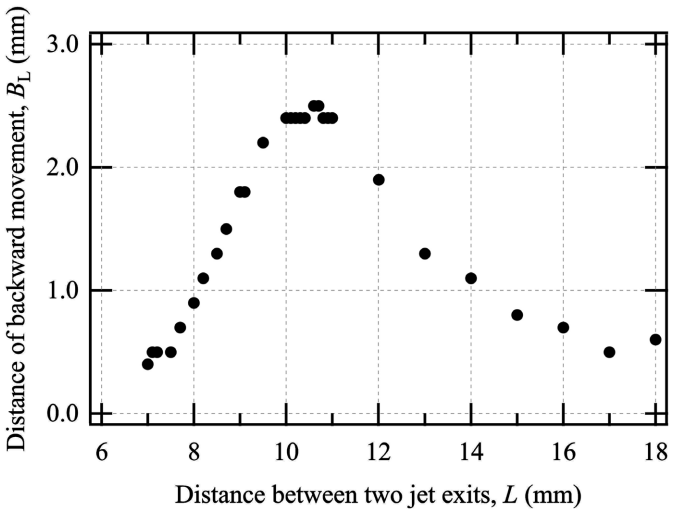

Figure 4. Distance of backward movement, B_L, as a function of distance between two jet exits, L.

Figure 6(a) and Figure 6(b) are the temporal evolution of the density distributions in single-jet conditions for Si and Ge, respectively. Si and Ge jets are injected from jet exits placed at $x = 0$ and 10 mm, respectively. The propagation direction of the shock wave is shown by the red arrow in the figure. Similarly to the $S_{Si}(t)$, the distance between the Ge jet exit and the shock front at t is denoted as $S_{Ge}(t)$. When two shock fronts collide at t for double-jet condition, the value of L corresponds to $S_{Si}(t) + S_{Ge}(t)$. As shown in Figure 6(a) and Figure 6(b), densities just behind the shock fronts increase with propagation until $t = t_4$ (560 ns), and the densities have maximum values at $t = t_4$. The evolution distances $S_{Si}(t_4)$ and $S_{Ge}(t_4)$ are both about 5 mm. This corresponds to $L \sim 10$ mm for the double-jet condition. These results indicate that B_L has a maximum value when the densities just behind the shock fronts for individual jets have maximum values. The density decreases with propagation after $t = t_5$. The time regimes until $t = t_4$ and after $t = t_5$ correspond to the growth and attenuation regimes of the

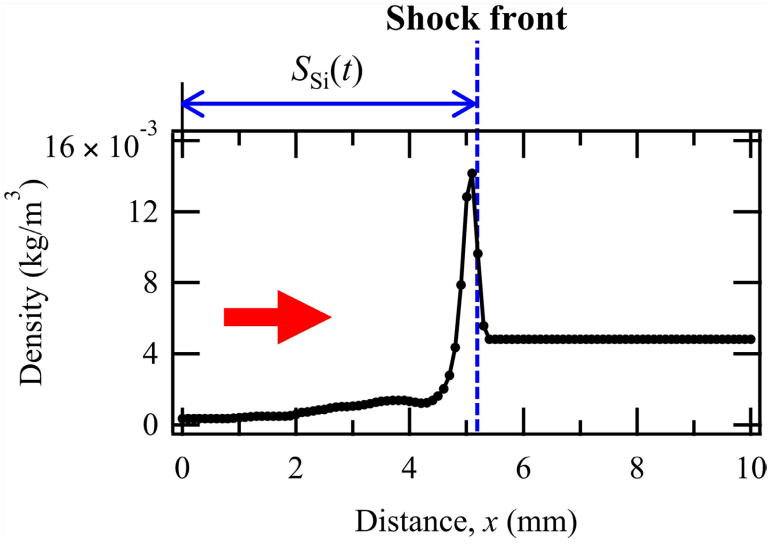

Figure 5. Density distribution for the single-jet condition for Si at $t = 560$ ns. The blue dashed line indicates the position of the shock front. Distance between Si jet exit and shock front, $S_{Si}(t)$, is denoted by the blue arrow.

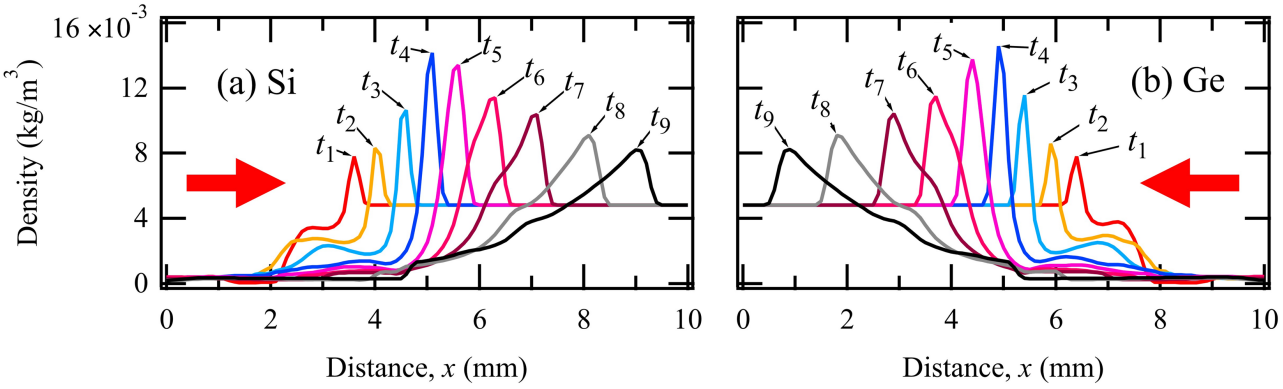

Figure 6. Time evolution of density distributions in single-jet conditions for (a) Si and (b) Ge. Time t_1, t_2, t_3, t_4, t_5, t_6, t_7, t_8 and t_9 are 250, 320, 430, 560, 730, 970, 1300, 1800 and 2400 ns, respectively.

shock wave, respectively. Hence, the origin of the increase of the distance of backward movement, B_L, until L = 10.7 mm is the head-on collision of the shock waves within their growth regime.

We discuss the effect of the collision of the shock waves within their growth regime on the distance of backward movement, B_L, by focusing on the flow in the interaction region. When two shock waves collide, the higher the density just behind the shock front, the higher the pressure in the interaction region. As a result, high-speed flow is induced just behind the shock front. The high-density and high-speed flow just behind the shock front formed during the growth of the shock wave are considered to lead the large B_L at around L = 10 mm. A more detailed analysis of the spatial distribution of density and velocity in the interaction region is necessary to understand the effect of the interaction region quantitatively.

5. Conclusion

Double pulsed-laser-ablation has been proposed as a method to prepare nanoparticle composites. The collision dynamics of two plumes is important to control the structure of composites. We numerically calculated the expansion dynamics of the oppositely injected Si and Ge jets into a He background gas as a simulation of double pulsed-laser-ablation. The experimentally observed backward movement of the jet after the collision with the counter-propagating shock front was reproduced. We quantitatively evaluated the effect of collision by defining the distance of backward movement, B_L. The value of B_L does not monotonically decrease with the distance between two jet exits, but has a peak at L = 10.7 mm in our calculation condition. We calculated the expansion feature of Si and Ge jets individually to discuss the origin of the peak. Shock wave grows with time at the initial stage of the jet expansion, and then attenuates. The density just behind the shock front for individual jet has a peak when the propagation distance of the shock front is about 5 mm and the time after the jet injection is 560 ns. They correspond to L ~10 mm for the collision of two shock waves. At this distance, a high-density interaction region is formed in the central region, and the value of B_L has a maximum for the double-jet condition. In the interaction region, the value of B_L is considered to be large due to the high density and high velocity. A more detailed analysis of the spatial distribution of density and velocity in the interaction region is necessary to understand the effect of the interaction region quantitatively. We found that the collision time and position of the two jets are important for the effects of counter-propagating shock waves on the plume expansion. They can be tuned by varying the distance between the exits of the two jets. The results of the calculation are helpful to determine the distance between the targets of double pulsed-laser-ablation.

Acknowledgements

This work was supported by JSPS KAKENHI Grant Number JP 22K04882.

Conflicts of Interest

The authors declare no conflicts of interest regarding the publication of this paper.

References

[1] Yamada, Y., Orii, T., Umezu, I., Takeyama, S.T.S. and Yoshida, T.Y.T. (1996) Optical Properties of Silicon Nanocrystallites Prepared by Excimer Laser Ablation in Inert Gas. *Japanese Journal of Applied Physics*, **35**, 1361. https://doi.org/10.1143/JJAP.35.1361

[2] Geohegan, D.B., Puretzky, A.A., Duscher, G. and Pennycook, S.J. (1998) Time-Resolved Imaging of Gas Phase Nanoparticle Synthesis by Laser Ablation. *Applied Physics Letters*, **72**, 2987-2989. https://doi.org/10.1063/1.121516

[3] Chrisey, D.B. and Hubler, G.K. (1994) Pulsed Laser Deposition of Thin Films. John Wiley & Sons Inc., Hoboken.

[4] Bäuerle, D. (2000) Laser Processing and Chemistry. Springer, Berlin.

[5] Umezu, I., Nakayama, Y. and Sugimura, A. (2010) Formation of Core-Shell Structured Silicon Nanoparticles during Pulsed Laser Ablation. *Journal of Applied Physics*, **107**, 094318. https://doi.org/10.1063/1.3374660

[6] Katayama, K., Horai, Y., Fukuoka, H., Kinoshita, T., Yoshida, T., Aoki, T. and Umezu, I. (2018) Effect of Counter Shock Wave on the Expanding Plume. *Applied Physics A*, **124**, Article Number: 150. https://doi.org/10.1007/s00339-018-1577-6

[7] Katayama, K., Kinoshita, T., Okada, R., Fukuoka, H., Yoshida, T., Aoki-Matsumoto, T. and Umezu, I. (2022) Mixing of Laser-Induced Plumes Colliding in a Background Gas. *Applied Physics A*, **128**, Article Number: 1007. https://doi.org/10.1007/s00339-022-06136-1

[8] Kinoshita, T., Fukuoka, H. and Umezu, I. (2018) Numerical Analysis of Behavior on Opposing Unsteady Supersonic Jets in a Flow Field with Shields. *Materials Science Forum*, **910**, 96-101. https://doi.org/10.4028/www.scientific.net/MSF.910.96